Multiple Brain Sources Are Differentially Engaged in the Inhibition of Distinct Action Types

Mario Hervault, Pier-Giorgio Zanone, Jean-Christophe Buisson, Raoul Huys

Multiple brain sources are differentially engaged in the inhibition of distinct action types

Mario Hervault[1], Pier-Giorgio Zanone[1], Jean-Christophe Buisson[2], Raoul Huys[1]

[1] Centre de Recherche Cerveau et Cognition - UMR 5549 CNRS - Université Toulouse 3 Paul Sabatier - 31000 Toulouse - France

[2] Institut de Recherche en Informatique de Toulouse - UMR 5505 CNRS - Université Toulouse 3 Paul Sabatier - 31000 Toulouse - France

Corresponding author:

Mario Hervault

CNRS CERCO UMR 5549, Pavillon Baudot CHU Purpan

BP 25202 - 31052 TOULOUSE CEDEX

mario.hervault@cnrs.fr

Acknowledgements:

All authors approved the final submitted version. The authors wish to thank all participants in this research.

The authors declare no competing financial interests.

Abstract

Most studies contributing to identify the brain network for inhibitory control have investigated the cancelation of prepared-discrete actions, thus focusing on an isolated and short-lived chunk of human behavior. Aborting ongoing-continuous actions is an equally crucial ability but remains little explored. Although discrete and ongoing-continuous rhythmic actions are associated with partially overlapping yet largely distinct brain activations, it is unknown whether the inhibitory network operates similarly in both situations. Thus, distinguishing between action types constitutes a powerful means to investigate whether inhibition is a generic function. We, therefore, used independent component analysis (ICA) of EEG data and show that canceling a discrete action and aborting a rhythmic action rely on independent brain components. The ICA showed that a Delta/Theta-power increase generically indexed inhibitory activity, whereas N2 and P3 ERP waves did so in an action-specific fashion. The action-specific components were generated by partially distinct brain sources, which indicates that the inhibitory network is engaged differently when canceling a prepared-discrete action versus aborting an ongoing-continuous action. In particular, increased activity was estimated in precentral gyri and posterior parts of the cingulate cortex for action canceling, whereas an enhanced activity was found in more frontal gyri and anterior parts of the cingulate cortex for action aborting. Overall, the present findings support the idea that inhibitory control is differentially implemented according to the type of action to revise.

Keywords Response inhibition, cognitive control, motor control, EEG, source separation

Introduction

The ability to stop planned or ongoing actions, crucial in everyday life, depends on an inhibitory executive function. Research based on the stop-signal paradigm (Logan & Cowan, 1984; Verbruggen et al., 2019) linked action stopping to an "inhibitory network" including cortical areas, namely, inferior frontal cortex (IFC), pre-supplementary motor area (pre-SMA) and cingulate cortex, as well as subcortical structures. This inhibitory network acts downstream on the brain "action network" that generates action through cortical and subcortical activations (Apšvalka et al., 2020; Aron et al., 2016; Bari & Robbins, 2013; Stinear et al., 2009). In the stop-signal paradigm, the standard task used in the domain, this inhibitory network underlies the successful cancelation of discrete action, as revealed by EEG evoked N2 and P3 potentials and increasing power of Delta (1-3 Hz) and Theta (4-7 Hz) oscillations (e.g., Huster et al., 2013; Hynd et al., 2021). These frontocentral EEG patterns proved to correlate with action cancelation across various inhibition situations (Dutra et al., 2018; Waller et al., 2019; Wessel & Aron, 2014).

Notwithstanding, the fundamental distinction between discrete and continuous actions[1] may challenge a unitary apprehension of the inhibitory network, for these action types rely on distinct action control processes (Huys et al., 2008). Effectively, they constitute *homo sapiens*' main movement primitives and are associated with distinct timing (explicit versus implicit for discrete and rhythmic action, respectively) (Huys et al., 2008, 2010; Spencer

[1] Discrete actions, such as grasping an object, are delimited by moments without displacement (i.e., with zero velocity and acceleration). In contrast, continuous actions, such as walking, lack such recognizable endpoints and are typically rhythmic as they constitute (periodic) repetitions of particular events (Hogan & Sternad, 2007).

et al., 2003). Discrete actions entail wider brain activation, implicating both cortical (Lacosse et al., 2016; Schaal et al., 2004; Wiegel et al., 2020) and subcortical areas (Habas & Cabanis, 2008; Mink & Thach, 1991), than rhythmic actions. This distinction has been notably shown regarding activations within the primary motor cortex (M1), pre-SMA, cingulate and cerebellar cortices, as well as thalamus and globus pallidus. Part of this differentiated action network (pre-SMA, cingulate cortex) is engaged in generating the "brain's stopping signal" or is targeted (M1, thalamus and globus pallidus) by this signal through the indirect and hyperdirect cortico-basal pathways that implement the inhibitory activity (Aron et al., 2016; Diesburg & Wessel, 2021). These differences in neural implementation, identified as downstream targets of the inhibitory network, might require distinct inhibitory activity. Yet, most previous studies have focused on discrete action canceling, ignoring continuous action aborting, even though both actions are crucial to human adaptive behavior. Studying inhibitory control of both movement types thus constitutes a powerful strategy to examine the generality of executive control and has practical implications for human performances (Everitt et al., 2015).

In addition, the exclusive use of discrete actions in investigating action inhibition comes with some limitations. The statistical "horse-race model" on which the classic stop-signal paradigm relies (Logan & Cowan, 1984; Verbruggen et al., 2019) constraints the exploration of its neural underpinnings and their modulation in clinical disorders (Hervault et al., 2019; Morein-Zamir et al., 2006; Schultz et al., 2021). Several authors have proposed that continuous actions should be favored when investigating

action inhibition in clinical populations such as attention deficit hyperactivity disorder (Leontyev & Yamauchi, 2019; Morein-Zamir et al., 2008) and Parkinson's disease (Lofredi et al., 2021). Continuous movements also allow for direct comparison of proactive and reactive inhibitory processes (Schultz et al., 2021). However, although action inhibition can be investigated based either on discrete or continuous actions, no study has directly compared the brain mechanisms, hence sources, engaged in the inhibition of these common types of actions. At least, a recent study of Lofredi et al. (2021) showed that subthalamic nucleus (STN) deep brain stimulation impaired ongoing-rhythmic movement abortion through potential modulation of the activity within a "fronto-subthalamic inhibitory triangle" (i.e., connectivity between IFC, pre-SMA and STN, identified from MRI connectome analysis). This first neuroimaging study on aborting ongoing-continuous movement suggests that the engaged brain structures could belong to the same broad inhibitory network involved in discrete action canceling (Aron et al., 2016). Still, whether the same activity is engaged within this network to inhibit discrete and continuous action is a crucial question that remains unresolved. Indeed, the different brain networks engaged in discrete and rhythmic action might require different inhibition processes to be inhibited. In contrast, independently of the network that produces the action, a unitary inhibition process might suppress the corticospinal output for action inhibition.

The few studies investigating stopping enduring or continuous movements have documented the implication of neural correlates of discrete-action inhibition when aborting a sustained static contraction of the elbow (P3 ERP wave, Hatta et al., 2003) or a continuous drawing action (N2 ERP wave,

Sosnik et al., 2015). Other research showed that ERP correlates of discrete-action inhibition originate from the cingulate cortex in the inhibitory network (Enriquez-Geppert et al., 2010; Huster et al., 2010), which is also engaged, but distinctly so, in discrete and continuous actions (Habas & Cabanis, 2008; Schaal et al., 2004). It is thus plausible that (some) EEG correlates of inhibition would indicate a dissociation of the inhibitory network activity as a function of the two action types.

In the present study, we investigated this issue using the inferential tool of EEG independent component analysis, based on the "common independent process identification" (CIPI) approach introduced by Wessel (2018). Blind source separation procedures enable decomposing EEG data into independent components that relate putatively to different psychological processes (Onton et al., 2006). By examining whether stop signals for distinct action types modulate similar brain components, we evaluated the commonality of the inhibitory network activity in canceling prepared-discrete actions and aborting ongoing-continuous (rhythmic) actions. This approach has been previously used to probe inhibitory control (e.g., Castiglione et al., 2019; Wessel et al., 2016) and is adopted here to disentangle the brain sources involved in inhibiting the two types of action.

Methods

Participants

Fourteen healthy individuals (8 males, mean age 25 years, SD = 2.2) served as voluntary participants. As assessed by the Edinburgh Handedness Inventory (Oldfield, 1971), all were right-handed and had a normal or corrected-to-normal vision. None of the participants reported a history of psychiatric or neurological disorders. The study was conducted according to the principles stated in the Declaration of Helsinki and the local research ethics committee approved the procedures (ID-RCB: 2020-A03215-34).

General procedure

Participants performed two experiments involving discrete or rhythmic movements execution. Both experiments were performed on the same WACOM Cintiq 15X tablet (1280×800-pixel resolution). As long as the stylus touched the tablet, the *x* and *y* coordinates of the performed movements were digitized at a sampling frequency of 143 Hz. The program controlling the tablet was custom-made.

Initial state

In the discrete experiment, at the beginning of each trial, participants adopted a static position (i.e., no movement), which consisted in keeping the stylus between two vertical yellow bands (1 mm wide, 10 mm distant) plotted at the center of the digitizing black screen. In the rhythmic experiment, participants were initially instructed to continuously oscillate at a spontaneous frequency (i.e., rhythmic movement) with the stylus between the two sides of the screen but with the oscillation's extrema falling outside the two centered vertical lines. In both experiments, the participant's arm

was fixed on the table to restrain the movement to the wrist articulation and avoid large muscular noise in the EEG signal due to intense contraction of the biceps and deltoid muscles.

Primary task

Primary-task stimuli were green or blue 50 ms flashes displayed on the whole tablet screen. In the discrete experiment, participants were instructed to reach with the stylus to the right versus left half-side of the tablet screen when a green versus blue flash appeared, respectively. As a reminder of the task, green and blue stickers were visible on the right and left sides of the tablet (**Fig.1**). The primary discrete task consisted of a two-choice reaction time involving a discrete-action response (GO_D condition). In the rhythmic experiment, the primary task was to pursue the rhythmic movement without interruption when the green and blue stimuli appeared ($CONTINUE_R$ condition).

Secondary task

In 25 % of the trials, the primary-task stimulus was followed by a red 50 ms flash, which indicated the participants to suppress their primary-task response. Thus, the secondary task required either to cancel the prepared discrete movement ($CANCEL_D$ condition) or to abort the ongoing rhythmic movement ($ABORT_R$ condition). Following $ABORT_R$ trials, a rhythmic GO_R trial was added to reengage participants in the rhythmic movement. In these GO_R trials, participants were instructed to transit from a static position to an oscillating movement as soon as the GO stimulus (green or blue) was presented. In the discrete experiment, the STOP-signal delay between the primary-task stimulus and the STOP signal (SSD), initially set to 200 ms, was

dynamically adjusted in 50 ms increments to achieve a probability of responding p(respond|signal) of .50. When the participant crossed a vertical line, the $CANCEL_D$ trial was considered a cancel-failure and the SSD was shortened; when the participant kept the stylus between the two lines, the $CANCEL_D$ trial was considered successful and the SSD was prolonged. In the rhythmic experiment, the SSD value was fixed at the value equivalent to the mean SSD obtained by each participant in the discrete experiment. All participants completed the discrete experiment one week prior to the rhythmic one.

In both experiments, the participants completed one practice block and 30 experimental blocks, each consisting of 20 trials. The discrete experiment was set up according to the standard guideline for STOP-signal experiments (Verbruggen et al., 2019). The rhythmic experiment design was close to the discrete one in terms of sensory stimulations and movement effector in order to limit the difference between the two experiments to the movement type involved in the main task (i.e., discrete or rhythmic).

EEG recording and preprocessing

EEG recordings were performed using an ActiveTwo system (BioSemi Instrumentation, 64 electrodes) with a sampling rate of 2048 Hz. The EEG electrodes were cautiously positioned based on four anatomical landmarks (i.e., nasion, inion, and preauricular points) in accordance with the 5 % 10/20 international system (TCT, 2012). The same experimenter positioned the EEG cap and electrodes, based on the same measures and landmarks, between the two experimental sessions of a single participant. Additional electrodes were placed below and above each eye. The data were online referenced to

the BioSemi CMS-DRL reference. All offsets from the reference were kept below 15 mV. The EEG data were filtered online with a band-pass frequency of 0.5-150 Hz. Continuous EEG data were imported and preprocessed in bespoke scripts using functions from the EEGLAB Matlab plugin (Delorme & Makeig, 2004). Visual inspection was used to remove channels with prominent artifacts in the continuous EEG. The EEG data were then re-referenced to a common average. The data were next partitioned into epochs of 1.6 s (locked to the primary stimulus onset; -400 ms to 1200 ms). Epochs containing values exceeding the average of the probability distribution of values across the data segments by 5 SD were rejected.

Experimental design and statistical analysis

Behavioral analysis

In both experiments, STOP-signal reaction times (SSRT) were computed in $CANCEL_D$ and $ABORT_R$ conditions to assess the inhibitory performance. For the discrete experiment, the participant's $SSRT_D$ was estimated using the integrative method (Verbruggen & Logan, 2009). This consisted in subtracting the mean SSD from the n^{th} reaction time (RT), where *n* equals the number of primary-stimulus RTs multiplied by the overall p(respond|signal). The main-stimulus RT in GO_D condition was calculated as the time between the stimulus onset and the response onset, the latter being defined as the moment the stylus motion had exceeded 5 % of the Euclidean distance between the initial and furthest (i.e., end) position of the discrete-movement response. In the rhythmic experiment, $SSRT_R$ was computed in each $ABORT_R$ trial using the rhythmic movement deviation method (Hervault et al., 2019). Briefly, $SSRT_R$ was calculated as the latency between the STOP signal onset and the onset of the response adjustment. This time point was defined as the moment the ongoing trajectory in phase space (i.e., the space spanned by *x* and *dx/dt*) deviated relative to movements without a STOP signal according to statistical criteria based on a sample's position in phase space, and the angle and magnitude of its corresponding velocity vector.

Overall CIPI procedure

EEG analyses were performed to test whether the inhibitory activity triggered by the STOP signal for prepared-discrete action canceling and ongoing rhythmic movement aborting involved the same brain component. A Common Independent Process Identification (CIPI) approach (Wessel, 2018)

was carried out according to the following steps (**Fig. 1**). First, the preprocessed EEG data from the two experiments were concatenated and submitted to a single decomposition using the infomax algorithm (Bell & Sejnowski, 1995; Makeig et al., 1996) for each participant. In the original scalp 64-channel data, each row of the data matrix represents voltage, summed between source projections to one data channel. After decomposition (63 components), each row of the data matrix gives the time course of the activity of one component process spatially filtered from the channel data (Delorme & Makeig, 2004). Second, non-brain components were removed from the data, that is, components with less than 10 % chance to account for neural activity as detected by the ICLABEL algorithm (Pion-Tonachini et al., 2019). The remaining components were fitted with individual inverse dipole-solutions using the DIPFIT algorithm (Oostenveld & Oostendorp, 2002). Components with non-dipolar equivalent dipole solutions usually represent non-brain signals (as defined by a residual variance of their equivalent dipole solution being greater than 15 %, Delorme et al., 2012), and were also removed. Third, one component was selected for each participant (IC-D) as the component which best reflected the STOP-signal-related activity in the discrete experiment (see below). Fourth, the capacity of this IC-D to reflect the STOP-signal-related activity in the rhythmic experiment was tested (see below). Fifth, conversely, an IC-R was similarly identified in the rhythmic experiment for each participant and then tested in the discrete one.

ERP and ERSP computation

To later select the components of interest, component-level event-related potentials (ERP) were computed for each participant in the two experiments' primary and secondary tasks. Event-related spectral perturbations (ERSP) were also computed. In the time-domain analysis, and for each of the 63 components, time-series locked to the primary stimulus onset were averaged across trials, following the subtraction of a −200 to 0 ms pre-stimulus period as baseline, to calculate ERP for GO_D and $CONTINUE_R$ conditions. For $CANCEL_D$ and $ABORT_R$ conditions, the ERP was re-aligned to the STOP-signal onset. For the frequency-domain analysis, the 63 component time series were convolved with complex 3-to-8 cycle-long Morlet's wavelets to compute the ERSP. Spectral power was estimated for each condition (1 to 50 ± 0.5 Hz, linearly spaced) as the absolute of the resulting coefficients for each frequency (normalized with respect to a −200 to 0 ms pre-stimulus baseline and transformed to decibel scale), and next averaged over trials. For the $CANCEL_D$ and $ABORT_R$ conditions, the spectral power locked to the primary-task stimulus was then subtracted from the spectral power in the GO_D and $CONTINUE_R$ conditions, respectively.

IC-D selection from $CANCEL_D$ condition and testing in $ABORT_R$ condition

One single component per participant, representing the inhibitory activity in the discrete experiment, was chosen as the IC-D in order to disentangle this activity from other neural and non-neural activities in the EEG. Whereas multiple components could, in principle, relate to inhibitory activity, the first component is most potent to investigate whether inhibitory activity in the discrete experiment is similarly engaged in the rhythmic experiment, and inversely. In addition, restricting the focus of investigation on one single

component significantly increases the signal-to-noise ratio of the underlying process of interest (Wessel, 2018; Wessel & Ullsperger, 2011). In order to select the component that best matched the inhibitory activity evoked by the STOP signal in the discrete experiment, we proceeded in three steps. First, since inhibitory processes are often discriminated by frontocentral activity over the scalp for both discrete (Huster et al., 2013) and continuous actions (Hervault et al., 2021; Sosnik et al., 2015), the topographical representation of the scalp-back projected IC had to reach its extrema at the frontocentral EEG electrodes (F1, Fz, F2, FC1, FCz, F2, C1, Cz or C2). Second, the IC-ERP had to show a significant difference between the successful $CANCEL_D$ condition and the GO_D condition (e.g., Enriquez-Geppert et al., 2010), indicating its functional implication in discrete action canceling. The significance of the ERPs was assessed, for each single participant, by a permutation testing procedure (see below). Third, in the resulting components, IC-D was chosen as the component that maximized the difference between $CANCEL_D$ and GO_D conditions IC-ERPs. To quantify the ERP difference between the two conditions, we took the maximal absolute difference between the two whole-epoch ERPs.

In order to evaluate the ability of the chosen IC-Ds to disentangle the $CANCEL_D$ and GO_D conditions' ERPs at the group level, a permutation testing procedure was applied (see below). Then, to assess the functional significance of the IC-D in the rhythmic experiment, we similarly tested whether the IC-D activity could disentangle $ABORT_R$ and $CONTINUE_R$ conditions ERPs by a similar permutation analysis (see below).

Reciprocal analysis

The same procedure was applied reciprocally to test the ability of the IC-R, selected from $ABORT_R$ versus $CONTINUE_R$ conditions in the rhythmic experiment, to differentiate the EEG activity between $CANCEL_D$ and GO_D conditions in the discrete experiment.

Statistical permutation testing

To compare components' activity between conditions at the group level, ERPs were subjected to a non-parametric permutation procedure (Maris & Oostenveld, 2007). The 14 participants' whole-epoch IC-ERPs were pooled over the two conditions (14 by conditions). Two sets of 14 ERPs each were then drawn randomly from this pool, and the differential grand-average ERP was computed between the two sets. This procedure was repeated 10 000 times, thus producing a distribution of these ERPs based on shuffled data under the null hypothesis. For each time point, a *p*-value was computed as the proportion of these pseudo-differential ERPs that exceeded the observed participants' average differential ERP. This *p*-value thus indicates at which time point the observed power distribution for the two conditions are more divergent than expected for random data ($p = .05$ threshold). To correct for multiple comparisons, we analyzed the resulting distributions of *p*-values to compute *p*-thresholds corresponding to the 2.5th percentile of the smallest, and the 97.5th percentile of the largest *p*-values distribution (Cohen, 2014). The same procedure was applied between trials of each participant in the IC selection procedure (see above). This permutation analysis was similarly applied to each time-frequency point to assess the ERSP significance in the different conditions.

Note that the CIPI approach has previously been used mainly to identify common neural mechanisms between task contexts (e.g., Castiglione et al., 2019; Wessel et al., 2016; Wessel & Aron, 2014), whereas here it was to show a disjunction between neural networks implicated in two different inhibition tasks. In this context, the disjunction approach requires appropriate precautions to avoid type-2 errors (Wessel, 2018). In order to show that a component related to one task is not involved in another, Wessel and Aron (2014) used a more liberal significance threshold of $p = .20$ to account for the type-2 error probability. Accordingly, we used a threshold of $p = .05$ to assess ERP significance when testing IC-D in the discrete task, whereas we used a threshold of $p = .20$ when testing IC-D in the rhythmic experiment and reciprocally for IC-R analysis.

Brain sources reconstruction

The CIPI procedure tests for the presence of IC-D activity in the rhythmic experiment and, inversely, for IC-R activity in the discrete one. Following this analysis, we compared the estimated brain areas recruited in the two experiments based on their corresponding representative ICs (i.e., IC-D for the $CANCEL_D$ condition and IC-R for the $ABORT_R$ one). For the source localization of the ICs, the inverse ICs weight projections onto the original EEG channels were exported to the sLORETA (standardized low-resolution brain electromagnetic tomography) data processing module (Pascual-Marqui, 2002). sLORETA provides a unique solution to the inverse problem (Marco-Pallarés et al., 2005; Pascual-Marqui, 2002; Sekihara et al., 2005). For sLORETA, the intracerebral volume is partitioned into 6239 voxels with a 5 mm spatial resolution. Then, the standardized current density at each voxel

has been calculated in a realistic head model (Fuchs et al., 2002) based on the MNI152 template due to the unavailability of individual participants' MRI scans.

[Fig. 1]

Results

Behavioral results

In the discrete experiment, basic requirements for the race-model application (Verbruggen et al., 2019) were fulfilled as main-stimulus (i.e., GO_D) RT was significantly longer for GO_D trials than for failed $CANCEL_D$ trials (paired t-test, $t = 9.30$, $p < .001$) and the 14 participants' overall p(respond|signal) was not significantly different from .50 ($t = 1.85$, $p > .05$). These results validate the computation of $SSRT_D$ (M = 269 ms, SD = 45 ms) in accordance with the model. In the rhythmic experiment, the spontaneous oscillation frequency was 1.62 Hz on average (SD = 0.49 Hz). To ensure that participants did not proactively anticipate the STOP signal occurrence, we tested whether the movement was slow down at the SSD latency (Schultz et al., 2021). Including all the $ABORT_R$ trials of our participants, we compared the movement mean velocity of the 100 ms time window surrounding the STOP signal occurrence (-50 ms to + 50 ms) to the movement mean velocity of the 100 ms time window surrounding the CONTINUE stimulus occurrence. This comparison (paired t-test) failed to show a significant difference between the two time windows for both the x-velocity ($t_{(2004)} = 0.28$, $p > .70$) and y-velocity ($t_{(2004)} = 0.07$, $p > .90$), indicating that the participants did not adapt the movement, proactively, in either movement's dimension. Measured $SSRT_R$ values (M = 268 ms, SD = 24 ms) did not differ from the $SSRT_D$ estimates (one-way ANOVA, $F = .02$, $p > .05$). The inhibition times of both experiments were unrelated across the 14 participants (Pearson correlation, $r = .02$, $p > .05$).

IC-D selection in the discrete experiment

According to the above-described procedure, one component per participant was retained; the grand-average characteristics of these IC-D components are shown in **Fig.2**.

The differential ERSP ($CANCEL_D$ minus GO_D trials) showed a significant post-STOP-signal increase in the Delta/Theta frequency range (**Fig.2 B**). The ERPs of the chosen IC-Ds demonstrated clear P3 wave evoked by the STOP signal, which significantly distinguish GO_D and $CANCEL_D$ conditions in the 318 - 559 ms time window (permutation test, $p < .05$, corrected for multiple comparisons, **Fig.2. A**) but did not show any N2 activity. The differential ERP was further tested for correlation across participants with the behavioral inhibition latency. The P3 peak amplitude was computed by looking for the maximal value in the 250-550 ms time range. P3 onset latency was defined as the time when half of the P3 peak amplitude value was reached. Pearson correlation across the 14 participants showed a significant correlation between $SSRT_D$ and both and P3 peak amplitude ($r = -.79$, $p < .001$, **Fig.3. A**) and P3 onset latency ($r = .78$, $p < .001$, **Fig.3. B**), indicating that an extensive and early P3 wave was associated with a shorter $SSRT_D$. P3 peak amplitude was also positively correlated to the ERSP peak (maximal value of the ERSP map within the significant region; $r = .62$, $p < .05$), indicating that a large evoked P3 amplitude was associated with an evoked high power in the Delta/Theta frequency range.

In addition to the functional relevance of the chosen IC-D, assessed by the correlations between the IC-D ERP measures and $SSRT_D$, we investigated IC-D relevance at the scalp-channel level. First, the EEGLAB *pvaf* function indicated that IC-D was, on average, explaining 11.88 % (SD = 5.40 %) of the

total scalp (64-channel) variance in the 600ms following the STOP signal occurrence in the $CANCEL_D$ condition and 54.48 % (SD = 15.20 %) when considering the frontocentral FCz site solely. Second, following Waller et al. (2019) logic, we compared the frontocentral channel-ERP (FCz site) between GO_D and $CANCEL_D$ conditions after back-projecting all non-artifact ICs, IC-D solely, or all ICs but IC-D. The results (**Fig.4 A**) suggested that most of the scalp-frontocentral difference between the two conditions was accounted for by the IC-D.

[Fig. 2]

[Fig. 3]

IC-D testing in the rhythmic experiment

Each participant's chosen IC-D component was then analyzed in the rhythmic experiment, with the same statistical procedure. The grand-average characteristics of these IC-D components are also shown in **Fig.2**. The differential ERSP ($ABORT_R$ minus $CONTINUE_R$ trials) showed a significant increase in the Delta/Theta frequency band in a similar time range as in the discrete experiment (**Fig.2 C**). However, the IC-D ERP was unable to significantly disentangle $CONTINUE_R$ and $ABORT_R$ conditions (permutation test, $p > .20$, **Figure 2.D**), even at a liberal threshold of $p = .20$. Moreover, the differential ERP ($ABORT_R$ minus $CONTINUE_R$ condition) did not show any significant correlation between P3 measures and the 14 participant's $SSRT_R$ (P3 onset latency: $r = -.38$, $p > .20$, peak amplitude: $r = .03$, $p > .90$) nor with time-frequency values (P3 peak amplitude - ERSP peak: $r = .05$, $p > .80$).

This indicates that the discrete IC-D activation was significantly related neither to the rhythmic $SSRT_R$ nor to the Theta oscillations.

[Fig. 4]

IC-R selection in the rhythmic experiment

As for the discrete experiment, one component per participant was chosen in the rhythmic experiment according to the reciprocal procedure; the grand-average characteristics of these IC-R components are shown in **Fig.5**. The differential ERSP ($ABORT_R$ minus $CONTINUE_R$ trials) showed a significant post-STOP-signal increase in the Delta/Theta frequency range (**Fig.5 C**). The ERPs of the chosen IC-Rs showed both clear N2 and P3 waves evoked by the STOP signal, which significantly separated the $ABORT_R$ and $CONTINUE_R$ conditions in a 192 - 308 ms and a 406 - 556 ms time window, respectively (permutation test, $p < .05$, corrected for multiple comparisons, **Fig.5 D**). The differential ERP ($ABORT_R$ minus $CONTINUE_R$ trials) was further tested for correlation with behavioral inhibition latency. To this end, P3 peak amplitude and P3 onset latency were computed as previously described. N2 features were similarly computed, looking for the minimal value in a 150-350 ms time window. Pearson correlation across the 14 participants showed a significant relation between SSRT-R and P3 peak amplitude ($r = -.65$, $p < .01$, **Fig.3. C**), indicating that an extensive P3 wave was associated with a shorter $SSRT_R$. In contrast $SSRT_R$ values did not correlate with P3 onset latency ($r = -.25$, $p > .30$) or N2 features ($|r| < .20$, $p > .30$). P3 peak amplitude was also positively correlated, across participants, to the ERSP peak value ($r = .60$, p

< .05), indicating that an evoked high P3 peak amplitude was associated with an evoked high power in the Delta/Theta frequency range. ERSP peak value did not correlate with N2 peak amplitude (r = -.07, p > .80).

As for IC-D, we investigated IC-R relevance at the scalp-channel level. IC-R was, on average, explaining 8.36 % (SD = 3.72 %) of the total scalp (64-channel) variance in the 600ms following the STOP signal occurrence in the $ABORT_R$ condition and 32.00 % (SD = 16.51 %) when considering the frontocentral FCz site solely. Next, we compared the frontocentral channel-ERP (FCz site) between $CONTINUE_R$ and $ABORT_R$ conditions after back-projecting all non-artifact ICs, IC-R solely, or all ICs but IC-R. The results (**Fig.4 B**) suggested that most of the scalp-frontocentral difference between the conditions was accounted for by the IC-R.

[Fig. 5]

IC-R testing in the discrete experiment

Each participant's chosen IC-R component was next analyzed in the discrete experiment with the same statistical procedure. The grand-average characteristics of these IC-R components are shown in **Fig.5**. The differential ERSP ($CANCEL_D$ minus GO_D condition) showed a significant increase in the Delta/Theta frequency band in a similar time range as in the rhythmic experiment (**Fig.5 B**). However, the IC-R ERP was unable to significantly disentangle GO_D and $CANCEL_D$ conditions (permutation test, p > .20, **Fig.5 A**). Moreover, the differential ERP ($CANCEL_D$ minus GO_D condition) did not show any significant correlation between ERP measures and $SSRT_D$ (P3

measures: |r| < .10, p > .80; N2 measures: |r| < .20, p > .60) or time-frequency values (P3 peak amplitude - ERSP peak: r = .50, p = .07; N2 peak amplitude - ERSP peak: r = .06, p > .80). This indicates that the IC-R activation was not significantly related to $SSRT_D$ or Theta oscillations in the discrete experiment.

Brain sources reconstruction

The voxel-based sLORETA images were compared across the two experimental tasks using voxel-wise randomization paired *t*-tests with 5000 permutations, based on statistical non-parametric mapping. Estimated voxels with significant differences ($p < .01$, corrected for multiple comparisons) between contrasted conditions were located in the MNI-brain. Differences between ICs-D and ICs-R on statistical maps of the source analyses are displayed in **Table 1** and **Fig.6**. These analyses revealed a significantly higher current density estimated for IC-D in the frontocentral region, including the midcingulate cortex (MCC) and the medial portion of the frontal gyrus, with maximum current source density estimate at MNI [(x,y,z) −10, 0, 40; $t = 3.66$]. In contrast, the IC-R showed higher activation in the insula, the anterior cingulate cortex (ACC), and the anterior part of the frontal cortex (see **Table 1**).

[Fig. 6]

[Table 1]

Discussion

Prior work has established distinctive EEG patterns correlated to the activity of a brain inhibitory network when canceling a prepared discrete action. Here, we tested whether these EEG correlates indicate a similar inhibitory activity in the case of aborting an ongoing-continuous (rhythmic) action. We recorded EEG while participants performed two experiments calling either for discrete action canceling or for rhythmic action aborting. In both situations, behavioral inhibition latencies fell within the range observed in previously used stop-signal tasks (e.g., Castiglione et al., 2019; Enriquez-Geppert et al., 2010; Havas et al., 2020; Hervault et al., 2019). The SSRT values from the two experiments were not significantly correlated. Although our current sample size prohibits to firmly conclude the absence of a behavioral relation, this result replicates one previously reported in inhibitory tasks with a comparable design (Hervault et al., 2019). The CIPI analysis of the EEG data (Wessel, 2018) corroborated these results, as independent brain components engaged when canceling and aborting action revealed a partial dissociation in the brain sources engaged in the two experiments.

The component that best represented the inhibitory activity in the discrete experiment exhibited the by-now classic correlates of action inhibition, namely, increasing Delta/Theta power and a large evoked P3 wave. The relevance of this IC-D for inhibition was confirmed by the significant $SSRT_D$/P3 latency correlation across participants, in line with previous stop-signal task studies (Huster et al., 2020; Hynd et al., 2021; Wessel & Aron, 2015). Crucially, its inability to disentangle ERPs pertaining to the rhythmic $ABORT_R$ and $CONTINUE_R$ conditions revealed that the IC-D is functionally irrelevant in

aborting ongoing rhythmic movements. Thus, the brain component that was most involved in discrete-action canceling turned out to be irrelevant for rhythmic-action aborting. At the same time, the IC-R identified in the rhythmic task also exhibited a stop-signal related Delta/Theta increase, as well as N2 and P3 waves, but failed to separate the ERPs for discrete $CANCEL_D$ and GO_D conditions (in either N2 or P3 time ranges). Therefore, the brain component that was most involved in (rhythmic) action stopping was irrelevant for (discrete) action canceling. Based on the inferential logic of the CIPI analysis (Wessel, 2018; Wessel & Aron, 2014), the present study thus demonstrates that distinct brain components are involved in discrete-action canceling and rhythmic-action aborting.

In terms of ERPs, both IC-D and IC-R contained a stop signal-related P3, which correlated to their respective SSRT in the discrete and rhythmic experiments. The absence of a significant P3 when evaluating the IC-D activity in the rhythmic experiment or, inversely, the IC-R activity in the discrete one suggests that the P3 signature is specific to the engaged inhibition brain component. This pattern of findings indicates that P3 is a clear-cut neural marker of action inhibition in the context of stop-signal reactions (Fine et al., 2020; Hynd et al., 2021; Tatz et al., 2021; Wessel & Aron, 2015). In addition, an N2 wave was exclusively evoked by the IC-R in the rhythmic $ABORT_R$ but not in any other condition. This N2 exclusivity allows for two interpretations. First, if N2 is considered for indexing an inhibitory process (see Huster et al., 2013, 2020), it sets apart discrete-action canceling and rhythmic-action aborting. Second, if N2 is thought to reflect another cognitive process, such as the allocation of attention or conflict detection, this process is differentially involved in the two

experiments. Regarding the time-frequency correlates of inhibition, the stop signal-related Delta/Theta power increase pertained to the P3 amplitude of both IC-D in the discrete task and IC-R in the rhythmic one. However, a significant Delta/Theta power increase was also observed when testing IC-D in the rhythmic experiment and, inversely, IC-R in the discrete one, corroborating the non-specificity of this power correlate. Similarly, a theta power enhancement is known to relate to the recruitment of cognitive control across different types of conflicts in the stream of information processing (Nigbur et al., 2011). Taken together, our EEG analyses suggest that stop signal-related inhibitory activity is exerted by different brain components for discrete and rhythmic actions, leading to distinct scalp activities (N2/P3 ERP complex) between the two situations.

The dissociation, at least partial, suggested by the CIPI analysis raises the question of whether the brain sources involved in discrete-action canceling and rhythmic-action aborting reflect a comparable engagement of the inhibitory network. Several studies have successfully localized the generators underlying discrete-action inhibition EEG correlates. They identified N2 generators in the IFC and MCC regions (Bekker et al., 2005; Enriquez-Geppert et al., 2010; Huster et al., 2010; Nieuwenhuis et al., 2003). P3 was also generated by a deep source in MCC, as well as by precentral and midfrontal gyri (Huster et al., 2010; Kok et al., 2004; Ramautar et al., 2006). Theta power increase could also originate, in several cognitive control tasks, from the frontal lobe and MCC sources (Mitchell et al., 2008). Here, the significant differences between IC-D and IC-R estimated neural sources tap well into the inhibition generators commonly reported in EEG signatures, suggesting that the two sit-

uations might differ in how inhibition is implemented. Notably, IC-D showed higher activity in the precentral gyrus (BA 6, likely corresponding to the pre-SMA), while IC-R sources revealed higher ACC activity. These separately estimated activations in the inhibitory network echo previous fMRI dissociations found in the action network, with higher pre-SMA activations in discrete movements (Habas & Cabanis, 2008; Schaal et al., 2004) and specific ACC activation in continuous movements (Habas & Cabanis, 2008). One interpretation is that, rather than a clear-cut delineation of anatomical action and inhibition networks, action execution and inhibition are controlled by networks with partially identical brain areas. Consequently, these common denominators (the precentral gyrus versus ACC for discrete and rhythmic actions, respectively) are either engaged in a functionally different, context-dependent manner (action control, inhibition) or act as "final pathway" to exert the inhibitory control. Other parts of the inhibitory network showed higher activity related to either IC-D (in MCC) or IC-R (in anterior regions of the frontal gyri) brain sources. Taken together, these results suggest that distinct action types associated with distinct cognitive and cerebral activity require, to be inhibited, an action-specific engagement of the inhibitory network. To further delineate how the brain action network modulation has consequences in an action-dependent involvement of the inhibitory network and its EEG correlates, future investigations might combine EEG-fMRI acquisition of multiple action types.

In stop-signal tasks, conflict arises whenever infrequent stop responses must overcome the prepotency of frequent responses (Braver et al., 2001; Mirabella, 2014). Differences in N2, P3, and the underlying cingulate cortex

activity have been shown to reflect the level of conflict existing in distinct inhibitory contexts (Braver et al., 2001; Enriquez-Geppert et al., 2010). More specifically, the EEG correlates of inhibition were specifically evoked by a go stimulus, a no-go signal, and a stop signal, with underlying modulations in the MCC and the precentral cortices activity (Enriquez-Geppert et al., 2010; Huster et al., 2010). In our case, the finding that IC-R activity is higher in the anterior part of the cingulate cortex, whereas the IC-D activity is higher in its posterior part, may be linked to the exclusivity of the N2 occurrence in rhythmic-movement aborting. Indeed, the anterior region of the MCC has been identified as a major neural generator of N2, whereas its posterior part does so for P3 (Huster et al., 2010). Such modulations of the inhibitory network activity in discrete actions have been interpreted as differences in the conflict-related stages of the information processing (Enriquez-Geppert et al., 2010; Randall & Smith, 2011). In particular, the discrete and rhythmic actions have been associated with distinct control regimes, in an open-loop versus closed-loop fashion (Jeannerod, 1988) and based on explicit versus implicit time representations, respectively (Spencer et al., 2003). Thus, the two action types might engage distinct predictive brain activity regarding the expected sensory outcomes of the movement and, hence, influence the disruption related to an unexpected stop signal occurrence. This difference in the conflict induced by the stop signal might modulate the engagement of the inhibitory network. Further work manipulating both conflict level and action type is needed to clarify the functional relevance of inhibitory-sources dissociation in brain activity, for instance, by varying the requirement associated with the infrequent signal (i.e., ABORT, CONTINUE).

In addition, Schultz et al. (2021) have shown that proactive inhibitory control in aborting a rhythmic action is associated with a slowdown of the movement prior to the stop signal occurrence. We showed that it was not the case in our continuous Abort-task, suggesting that our results suggest reactive inhibition engagement. Still, further studies are necessary to establish how this proactive inhibition is implemented in the brain activity when aborting a continuous action and whether this activity is common to the brain activity related to the proactive inhibition engaged in canceling a discrete action (Elchlepp et al., 2016).

To conclude, the present findings showed that the inhibitory activity involved in discrete action canceling and rhythmic action aborting rely on partially dissociated brain sources. This dissociation suggests that the EEG patterns commonly related to stopping activity may reflect the involvement of distinct brain sources, differentially enrolled in the inhibitory network depending on the action type to revise. Therefore, assessing the commonality of inhibitory control across multiple, fundamentally distinct action types appears instrumental in providing a complete (neural) model of inhibitory control.

References

Apšvalka, D., Ferreira, C. S., Schmitz, T. W., Rowe, J. B., & Anderson, M. C. (2020). *Dynamic targeting enables domain-general inhibitory control over action and thought by the prefrontal cortex* [Preprint]. Neuroscience. https://doi.org/10.1101/2020.10.22.350520

Aron, A. R., Herz, D. M., Brown, P., Forstmann, B. U., & Zaghloul, K. (2016). Frontosubthalamic Circuits for Control of Action and Cognition. *The Journal of Neuroscience: The Official Journal of the Society for Neuroscience*, *36*(45), 11489–11495. https://doi.org/10.1523/JNEUROSCI.2348-16.2016

Bari, A., & Robbins, T. W. (2013). Inhibition and impulsivity: Behavioral and neural basis of response control. *Progress in Neurobiology*, *108*, 44–79. https://doi.org/10.1016/j.pneurobio.2013.06.005

Bekker, E. M., Kenemans, J. L., & Verbaten, M. N. (2005). Source analysis of the N2 in a cued Go/NoGo task. *Cognitive Brain Research*, *22*(2), 221–231. https://doi.org/10.1016/j.cogbrainres.2004.08.011

Bell, A. J., & Sejnowski, T. J. (1995). An information-maximization approach to blind separation and blind deconvolution. *Neural Computation*, *7*(6), 1129–1159. https://doi.org/10.1162/neco.1995.7.6.1129

Braver, T. S., Barch, D. M., Gray, J. R., Molfese, D. L., & Snyder, A. (2001). Anterior cingulate cortex and response conflict: Effects of frequency, inhibition and errors. *Cerebral Cortex (New York, N.Y.: 1991)*, *11*(9), 825–836. https://doi.org/10.1093/cercor/11.9.825

Castiglione, A., Wagner, J., Anderson, M., & Aron, A. R. (2019). Preventing a Thought from Coming to Mind Elicits Increased Right Frontal Beta Just

as Stopping Action Does. *Cerebral Cortex*, *29*(5), 2160–2172. https://doi.org/10.1093/cercor/bhz017

Cohen, M. X. (2014). *Analyzing Neural Time Series Data – Theory and Practice* (1st ed.). MIT Press.

Delorme, A., & Makeig, S. (2004). EEGLAB: An open source toolbox for analysis of single-trial EEG dynamics including independent component analysis. *Journal of Neuroscience Methods*, *134*(1), 9–21. https://doi.org/10.1016/j.jneumeth.2003.10.009

Delorme, A., Palmer, J., Onton, J., Oostenveld, R., & Makeig, S. (2012). Independent EEG Sources Are Dipolar. *PLOS ONE*, *7*(2), e30135. https://doi.org/10.1371/journal.pone.0030135

Diesburg, D. A., & Wessel, J. R. (2021). The Pause-then-Cancel model of human action-stopping: Theoretical considerations and empirical evidence. *Neuroscience & Biobehavioral Reviews*, *129*, 17–34. https://doi.org/10.1016/j.neubiorev.2021.07.019

Dutra, I. C., Waller, D. A., & Wessel, J. R. (2018). Perceptual Surprise Improves Action Stopping by Nonselectively Suppressing Motor Activity via a Neural Mechanism for Motor Inhibition. *Journal of Neuroscience*, *38*(6), 1482–1492. https://doi.org/10.1523/JNEUROSCI.3091-17.2017

Elchlepp, H., Lavric, A., Chambers, C. D., & Verbruggen, F. (2016). Proactive inhibitory control: A general biasing account. *Cognitive Psychology*, *86*, 27–61. https://doi.org/10.1016/j.cogpsych.2016.01.004

Enriquez-Geppert, S., Konrad, C., Pantev, C., & Huster, R. J. (2010). Conflict and inhibition differentially affect the N200/P300 complex in a

combined go/nogo and stop-signal task. *NeuroImage*, *51*(2), 877–887. https://doi.org/10.1016/j.neuroimage.2010.02.043

Everitt, J., Fletcher, S., & Caird-Daley, A. (2015). Task analysis of discrete and continuous skills: A dual methodology approach to human skills capture for automation. *Theoretical Issues in Ergonomics Science*, *16*(5), 513–532. https://doi.org/10.1080/1463922X.2015.1028508

Fine, J. M., Fini, M. E., Mysore, A. S., Tyler, W. J., & Santello, M. (2020). Response inhibition is driven by top-down network mechanisms and enhanced with focused ultrasound. *BioRxiv*, 649665. https://doi.org/10.1101/649665

Fuchs, M., Kastner, J., Wagner, M., Hawes, S., & Ebersole, J. S. (2002). A standardized boundary element method volume conductor model. *Clinical Neurophysiology: Official Journal of the International Federation of Clinical Neurophysiology*, *113*(5), 702–712. https://doi.org/10.1016/s1388-2457(02)00030-5

Habas, C., & Cabanis, E. A. (2008). Neural correlates of simple unimanual discrete and continuous movements: A functional imaging study at 3 T. *Neuroradiology*, *50*(4), 367–375. https://doi.org/10.1007/s00234-007-0354-6

Hatta, A., Nishihira, Y., Kaneda, T., Wasaka, T., Kida, T., Kuroiwa, K., & Akiyama, S. (2003). Somatosensory event-related potentials (ERPs) associated with stopping ongoing movement. *Perceptual and Motor Skills*, *97*(3 Pt 1), 895–904. https://doi.org/10.2466/pms.2003.97.3.895

Havas, J. D., Ito, S., & Gomi, H. (2020). On stopping voluntary muscle relaxations and contractions: Evidence for shared control mechanisms

and muscle state specific active breaking. *Journal of Neuroscience*. https://doi.org/10.1523/JNEUROSCI.0002-20.2020

Hervault, M., Huys, R., Farrer, C., Buisson, J. C., & Zanone, P. G. (2019). Cancelling discrete and stopping ongoing rhythmic movements: Do they involve the same process of motor inhibition? *Human Movement Science*, *64*, 296–306. https://doi.org/10.1016/j.humov.2019.02.010

Hervault, M., Zanone, P.-G., Buisson, J.-C., & Huys, R. (2021). *Hold your horses: Differences in EEG correlates of inhibition in cancelling and stopping an action*. PsyArXiv. https://doi.org/10.31234/osf.io/ys9pd

Hogan, N., & Sternad, D. (2007). On rhythmic and discrete movements: Reflections, definitions and implications for motor control. *Experimental Brain Research*, *181*(1), 13–30. https://doi.org/10.1007/s00221-007-0899-y

Huster, R. J., Enriquez-Geppert, S., Lavallee, C. F., Falkenstein, M., & Herrmann, C. S. (2013). Electroencephalography of response inhibition tasks: Functional networks and cognitive contributions. *International Journal of Psychophysiology: Official Journal of the International Organization of Psychophysiology*, *87*(3), 217–233. https://doi.org/10.1016/j.ijpsycho.2012.08.001

Huster, R. J., Messel, M. S., Thunberg, C., & Raud, L. (2020). The P300 as marker of inhibitory control – Fact or fiction? *Cortex*. https://doi.org/10.1016/j.cortex.2020.05.021

Huster, R. J., Westerhausen, R., Pantev, C., & Konrad, C. (2010). The role of the cingulate cortex as neural generator of the N200 and P300 in a

tactile response inhibition task. *Human Brain Mapping*, *31*(8), 1260–1271. https://doi.org/10.1002/hbm.20933

Huys, R., Studenka, B. E., Rheaume, N. L., Zelaznik, H. N., & Jirsa, V. K. (2008). Distinct Timing Mechanisms Produce Discrete and Continuous Movements. *PLoS Computational Biology*, *4*(4), e1000061. https://doi.org/10.1371/journal.pcbi.1000061

Huys, R., Studenka, B. E., Zelaznik, H. N., & Jirsa, V. K. (2010). Distinct timing mechanisms are implicated in distinct circle drawing tasks. *Neuroscience Letters*, *472*(1), 24–28. https://doi.org/10.1016/j.neulet.2010.01.047

Hynd, M., Soh, C., Rangel, B. O., & Wessel, J. R. (2021). Paired-pulse TMS and scalp EEG reveal systematic relationship between inhibitory GABAa signaling in M1 and fronto-central cortical activity during action stopping. *Journal of Neurophysiology*, *125*(2), 648–660. https://doi.org/10.1152/jn.00571.2020

Jeannerod, M. (1988). *The neural and behavioural organization of goal-directed movements* (pp. xii, 283). Clarendon Press/Oxford University Press.

Kok, A., Ramautar, J. R., De Ruiter, M. B., Band, G. P. H., & Ridderinkhof, K. R. (2004). ERP components associated with successful and unsuccessful stopping in a stop-signal task. *Psychophysiology*, *41*(1), 9–20. https://doi.org/10.1046/j.1469-8986.2003.00127.x

Lacosse, E., Bause, J., Lohmann, G., Scheffler, K., Schaal, S., & Sternad, D. (2016). *Neural Control of Discrete and Rhythmic Movements*. 53–54.

https://pure.mpg.de/pubman/faces/ViewItemOverviewPage.jsp?itemId=item_2547327

Leontyev, A., & Yamauchi, T. (2019). Mouse movement measures enhance the stop-signal task in adult ADHD assessment. *PLOS ONE*, *14*(11), e0225437. https://doi.org/10.1371/journal.pone.0225437

Lofredi, R., Auernig, G. C., Irmen, F., Nieweler, J., Neumann, W.-J., Horn, A., Schneider, G.-H., & Kühn, A. A. (2021). Subthalamic stimulation impairs stopping of ongoing movements. *Brain*, *144*(1), 44–52. https://doi.org/10.1093/brain/awaa341

Logan, G. D., & Cowan, W. B. (1984). On the ability to inhibit thought and action: A theory of an act of control. *Psychological Review*, *91*(3), 295–327. https://doi.org/10.1037/0033-295X.91.3.295

Makeig, S., Bell, A., Jung, T. P., & Sejnowski, T. J. (1996). Independent component analysis of electroencephalographic data. *Advances in Neural Information Processing Systems*, 145–151.

Marco-Pallarés, J., Grau, C., & Ruffini, G. (2005). Combined ICA-LORETA analysis of mismatch negativity. *NeuroImage*, *25*(2), 471–477. https://doi.org/10.1016/j.neuroimage.2004.11.028

Maris, E., & Oostenveld, R. (2007). Nonparametric statistical testing of EEG- and MEG-data. *Journal of Neuroscience Methods*, *164*(1), 177–190. https://doi.org/10.1016/j.jneumeth.2007.03.024

Mink, J. W., & Thach, W. T. (1991). Basal ganglia motor control. I. Nonexclusive relation of pallidal discharge to five movement modes. *Journal of Neurophysiology*, *65*(2), 273–300. https://doi.org/10.1152/jn.1991.65.2.273

Mirabella, G. (2014). Should I stay or should I go? Conceptual underpinnings of goal-directed actions. *Frontiers in Systems Neuroscience*, *8*, 6. https://doi.org/10.3389/fnsys.2014.00206

Mitchell, D. J., McNaughton, N., Flanagan, D., & Kirk, I. J. (2008). Frontal-midline theta from the perspective of hippocampal “theta.” *Progress in Neurobiology*, *86*(3), 156–185. https://doi.org/10.1016/j.pneurobio.2008.09.005

Morein-Zamir, S., Chua, R., Franks, I., Nagelkerke, P., & Kingstone, A. (2006). Measuring online volitional response control with a continuous tracking task. *Behavior Research Methods*, *38*(4), 638–647. https://doi.org/10.3758/BF03193896

Morein-Zamir, S., Hommersen, P., Johnston, C., & Kingstone, A. (2008). Novel measures of response performance and inhibition in children with ADHD. *Journal of Abnormal Child Psychology*, *36*(8), 1199–1210. https://doi.org/10.1007/s10802-008-9243-7

Nieuwenhuis, S., Yeung, N., van den Wildenberg, W., & Ridderinkhof, K. R. (2003). Electrophysiological correlates of anterior cingulate function in a go/no-go task: Effects of response conflict and trial type frequency. *Cognitive, Affective & Behavioral Neuroscience*, *3*(1), 17–26. https://doi.org/10.3758/cabn.3.1.17

Nigbur, R., Ivanova, G., & Stürmer, B. (2011). Theta power as a marker for cognitive interference. *Clinical Neurophysiology: Official Journal of the International Federation of Clinical Neurophysiology*, *122*(11), 2185–2194. https://doi.org/10.1016/j.clinph.2011.03.030

Oldfield, R. C. (1971). The assessment and analysis of handedness: The Edinburgh inventory. *Neuropsychologia*, *9*(1), 97–113. https://doi.org/10.1016/0028-3932(71)90067-4

Onton, J., Westerfield, M., Townsend, J., & Makeig, S. (2006). Imaging human EEG dynamics using independent component analysis. *Neuroscience and Biobehavioral Reviews*, *30*(6), 808–822. https://doi.org/10.1016/j.neubiorev.2006.06.007

Oostenveld, R., & Oostendorp, T. F. (2002). Validating the boundary element method for forward and inverse EEG computations in the presence of a hole in the skull. *Human Brain Mapping*, *17*(3), 179–192. https://doi.org/10.1002/hbm.10061

Pascual-Marqui, R. D. (2002). Standardized low-resolution brain electromagnetic tomography (sLORETA): Technical details. *Methods and Findings in Experimental and Clinical Pharmacology*, *24 Suppl D*, 5–12.

Pion-Tonachini, L., Kreutz-Delgado, K., & Makeig, S. (2019). ICLabel: An automated electroencephalographic independent component classifier, dataset, and website. *NeuroImage*, *198*, 181–197. https://doi.org/10.1016/j.neuroimage.2019.05.026

Ramautar, J. R., Kok, A., & Ridderinkhof, K. R. (2006). Effects of stop-signal modality on the N2/P3 complex elicited in the stop-signal paradigm. *Biological Psychology*, *72*(1), 96–109. https://doi.org/10.1016/j.biopsycho.2005.08.001

Randall, W. M., & Smith, J. L. (2011). Conflict and inhibition in the cued-Go/NoGo task. *Clinical Neurophysiology*, *122*(12), 2400–2407. https://doi.org/10.1016/j.clinph.2011.05.012

Schaal, S., Sternad, D., Osu, R., & Kawato, M. (2004). Rhythmic arm movement is not discrete. *Nature Neuroscience*, *7*(10), 1136–1143. https://doi.org/10.1038/nn1322

Schultz, K. E., Denning, D., Hufnagel, V., & Swann, N. (2021). Stopping a Continuous Movement: A Novel Approach to Investigating Motor Control. *BioRxiv*, 2021.04.08.439070. https://doi.org/10.1101/2021.04.08.439070

Sekihara, K., Sahani, M., & Nagarajan, S. S. (2005). Localization bias and spatial resolution of adaptive and non-adaptive spatial filters for MEG source reconstruction. *NeuroImage*, *25*(4), 1056–1067. https://doi.org/10.1016/j.neuroimage.2004.11.051

Sosnik, R., Chaim, E., & Flash, T. (2015). Stopping is not an option: The evolution of unstoppable motion elements (primitives). *Journal of Neurophysiology*, *114*(2), 846–856. https://doi.org/10.1152/jn.00341.2015

Spencer, R. M. C., Zelaznik, H. N., Diedrichsen, J., & Ivry, R. B. (2003). Disrupted timing of discontinuous but not continuous movements by cerebellar lesions. *Science (New York, N.Y.)*, *300*(5624), 1437–1439. https://doi.org/10.1126/science.1083661

Stinear, C. M., Coxon, J. P., & Byblow, W. D. (2009). Primary motor cortex and movement prevention: Where Stop meets Go. *Neuroscience &*

Biobehavioral Reviews, *33*(5), 662–673. https://doi.org/10.1016/j.neubiorev.2008.08.013

Tatz, J. R., Soh, C., & Wessel, J. R. (2021). Common and unique inhibitory control signatures of action-stopping and attentional capture suggest that actions are stopped in two stages. *Journal of Neuroscience*. https://doi.org/10.1523/JNEUROSCI.1105-21.2021

Trans Cranial Technologies. (2012). *10/20 System Positioning Manual*. https://www.trans-cranial.com/docs/10_20_pos_man_v1_0_pdf.pdf

Verbruggen, F., Aron, A. R., Band, G. P., Beste, C., Bissett, P. G., Brockett, A. T., Brown, J. W., Chamberlain, S. R., Chambers, C. D., Colonius, H., Colzato, L. S., Corneil, B. D., Coxon, J. P., Dupuis, A., Eagle, D. M., Garavan, H., Greenhouse, I., Heathcote, A., Huster, R. J., … Boehler, C. N. (2019). A consensus guide to capturing the ability to inhibit actions and impulsive behaviors in the stop-signal task. *ELife*, *8*, e46323. https://doi.org/10.7554/eLife.46323

Verbruggen, F., & Logan, G. D. (2009). Models of response inhibition in the stop-signal and stop-change paradigms. *Neuroscience and Biobehavioral Reviews*, *33*(5), 647–661. https://doi.org/10.1016/j.neubiorev.2008.08.014

Waller, D. A., Hazeltine, E., & Wessel, J. R. (2019). Common neural processes during action-stopping and infrequent stimulus detection: The frontocentral P3 as an index of generic motor inhibition. *International Journal of Psychophysiology*. https://doi.org/10.1016/j.ijpsycho.2019.01.004

Wessel, J. R. (2018). Testing Multiple Psychological Processes for Common Neural Mechanisms Using EEG and Independent Component Analysis. *Brain Topography*, *31*(1), 90–100. https://doi.org/10.1007/s10548-016-0483-5

Wessel, J. R., & Aron, A. R. (2014). Inhibitory motor control based on complex stopping goals relies on the same brain network as simple stopping. *NeuroImage*, *103*, 225–234. https://doi.org/10.1016/j.neuroimage.2014.09.048

Wessel, J. R., & Aron, A. R. (2015). It's not too late: The onset of the frontocentral P3 indexes successful response inhibition in the stop-signal paradigm. *Psychophysiology*, *52*(4), 472–480. https://doi.org/10.1111/psyp.12374

Wessel, J. R., Jenkinson, N., Brittain, J.-S., Voets, S. H. E. M., Aziz, T. Z., & Aron, A. R. (2016). Surprise disrupts cognition via a fronto-basal ganglia suppressive mechanism. *Nature Communications*, *7*(1), 11195. https://doi.org/10.1038/ncomms11195

Wessel, J. R., & Ullsperger, M. (2011). Selection of independent components representing event-related brain potentials: A data-driven approach for greater objectivity. *NeuroImage*, *54*(3), 2105–2115. https://doi.org/10.1016/j.neuroimage.2010.10.033

Wiegel, P., Kurz, A., & Leukel, C. (2020). Evidence that distinct human primary motor cortex circuits control discrete and rhythmic movements. *The Journal of Physiology*, *598*(6), 1235–1251. https://doi.org/10.1113/JP278779

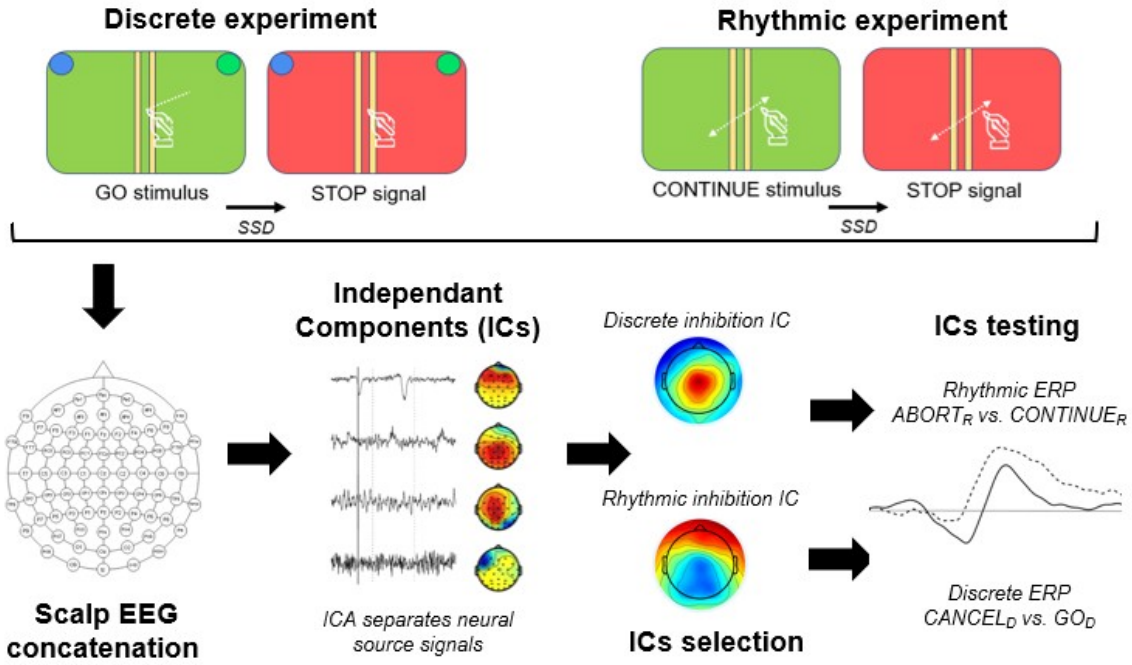

Fig.1: **EEG CIPI analysis overview**

The concatenated EEG from the discrete and rhythmic experiments were subjected to ICA. One IC that represented the process underlying inhibition in the discrete experiment was selected on a single participant basis. Subsequently, the capacity of that component to disentangle ABORT$_R$ versus CONTINUE$_R$ conditions in the rhythmic experiment was assessed. Reciprocally, ICs underlying rhythmic inhibition were selected and then tested in the discrete experiment to disentangle CANCEL$_D$ versus GO$_D$ conditions.

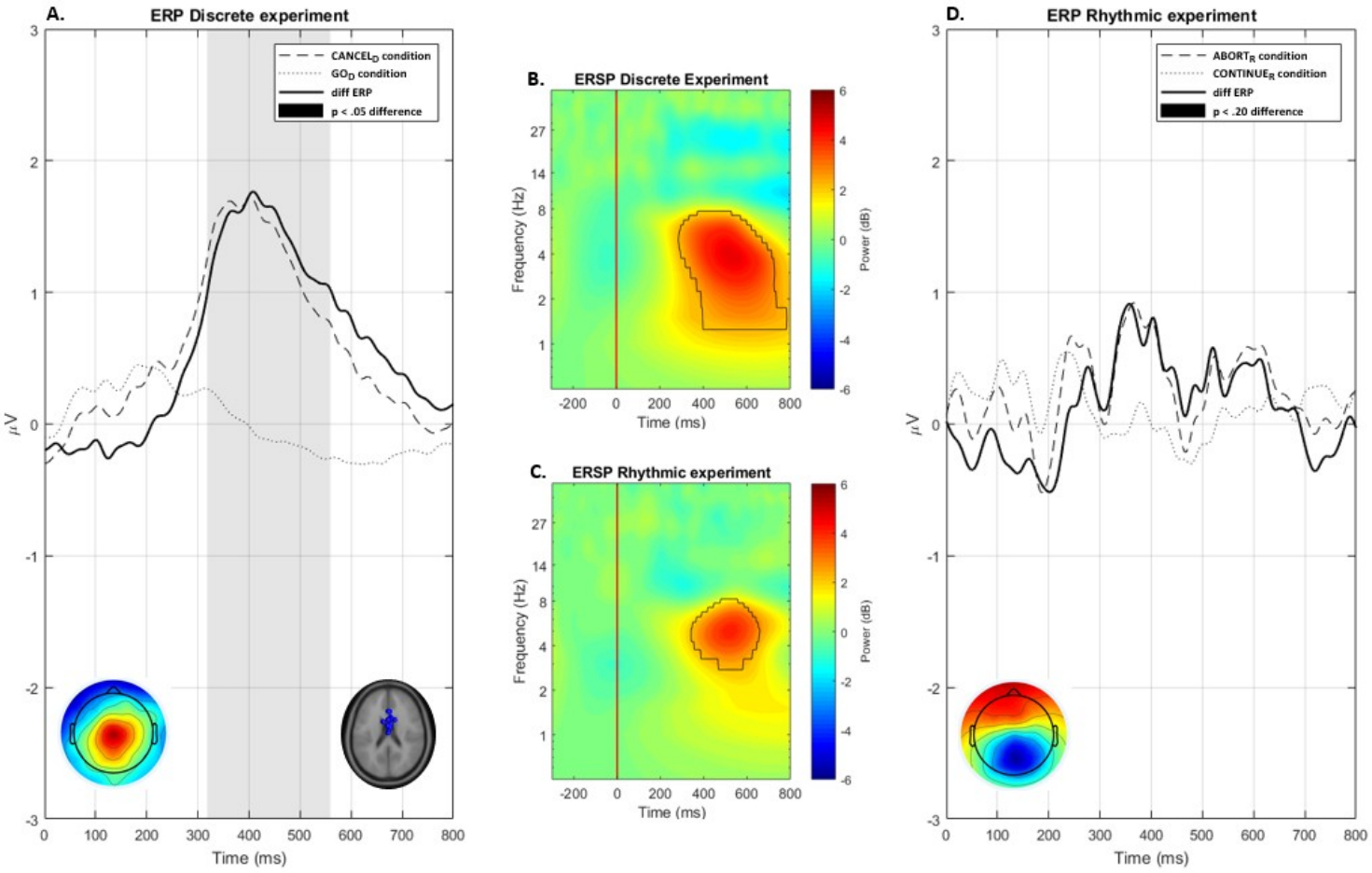

931

Fig.2: **Discrete chosen component (IC–D) analysis**

Panel A*: IC–D ERP (grand–average) in the discrete experiment, showing the difference between GO_D and $CANCEL_D$ conditions.* ***Panel D****: IC–D ERP (grand–average) in the rhythmic experiment, showing difference between $CONTINUE_R$ and $ABORT_R$ conditions. $CANCEL_D$ and $ABORT_R$ conditions topographical maps of the IC–D components were computed in the channel space at the P3 peak latency. Equivalent current dipole model of the participants' IC–Ds is also portrayed.*

Panel B–C*: IC–D ERSP maps computed in the discrete $CANCEL_D$ (B) and rhythmic $ABORT_R$ (C) conditions. Red line: STOP signal occurrence. Black contour line: region of significant activation ($p < .05$, corrected for multiple comparisons).*

89
90

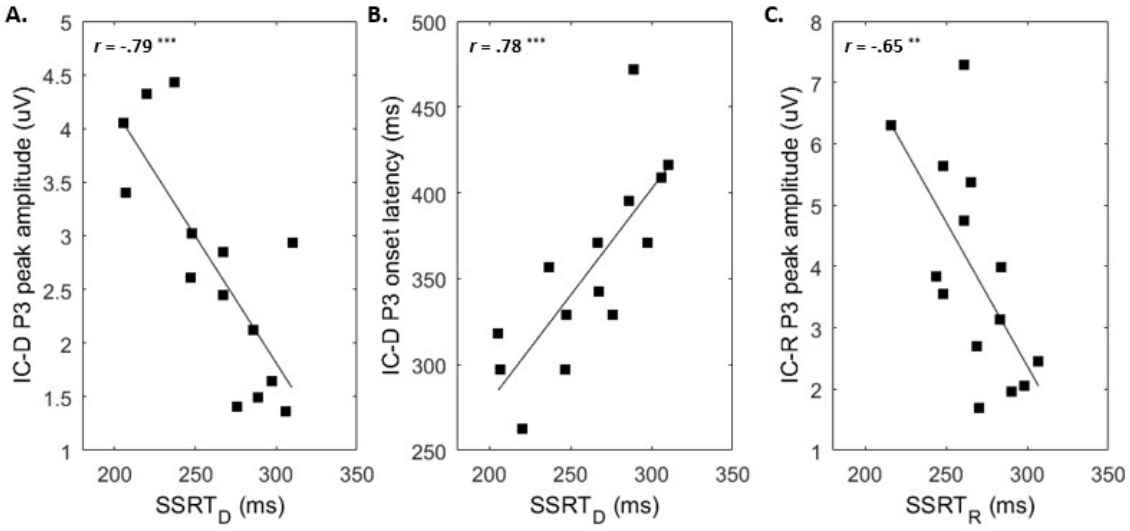

Fig.3: IC ERPs - Behavior correlations

***Panel A**: IC-D P3 peak amplitude correlation with $SSRT_D$. **Panel B**: IC-D P3 peak amplitude correlation with $SSRT_D$. **Panel C**: IC-R P3 peak amplitude correlation with $SSRT_R$.*

**** p < .001, ** p < .01, * p < .05*

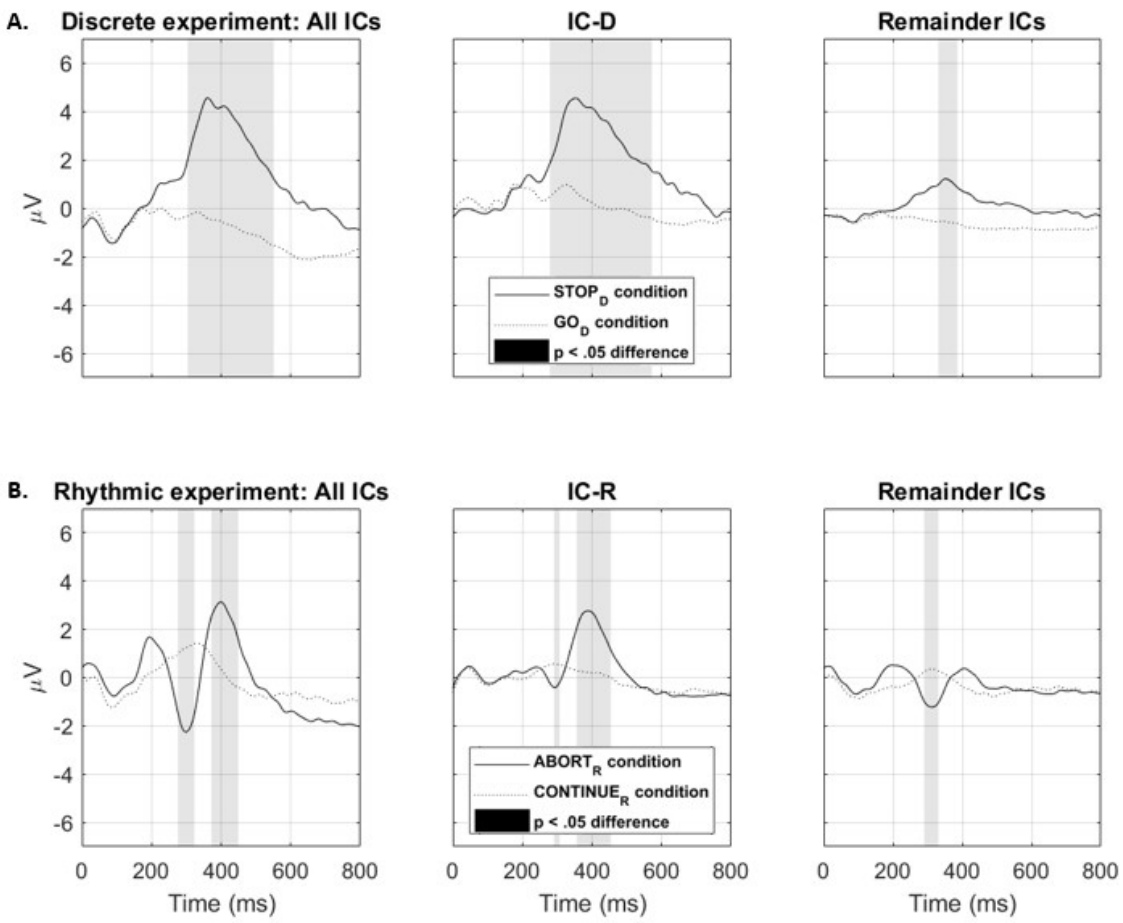

Fig.4: IC-D and IC-R back-projection at the frontocentral channel level

***Panel A**: Scalp FCz STOP-signal locked ERP in the discrete GO_D and $CANCEL_D$ conditions after back-projecting all non-artefact ICs, IC-D solely, or all ICs but IC-D. The two conditions differed significantly (non-parametric permutation procedure, p <.05, corrected for multiple comparisons) for the All-ICs projection (304 to 551 ms), the IC-D solely (275 to 572 ms) and the remaining ICs (331 to 386 ms) projections.*

***Panel B**: Scalp FCz STOP-signal locked ERP in the rhythmic $CONTINE_R$ and $ABORT_R$ conditions after back-projecting all non-artefact ICs, IC-R solely, or all ICs but IC-R. The two conditions differed significantly (non-parametric permutation procedure, p <.05, corrected for multiple comparisons) for the All-ICs projection (276 to 323 ms, 372 to 449 ms), the IC-R solely (291 to 307 ms, 356 to 454 ms) and the remaining ICs (290 to 331 ms) projections.*

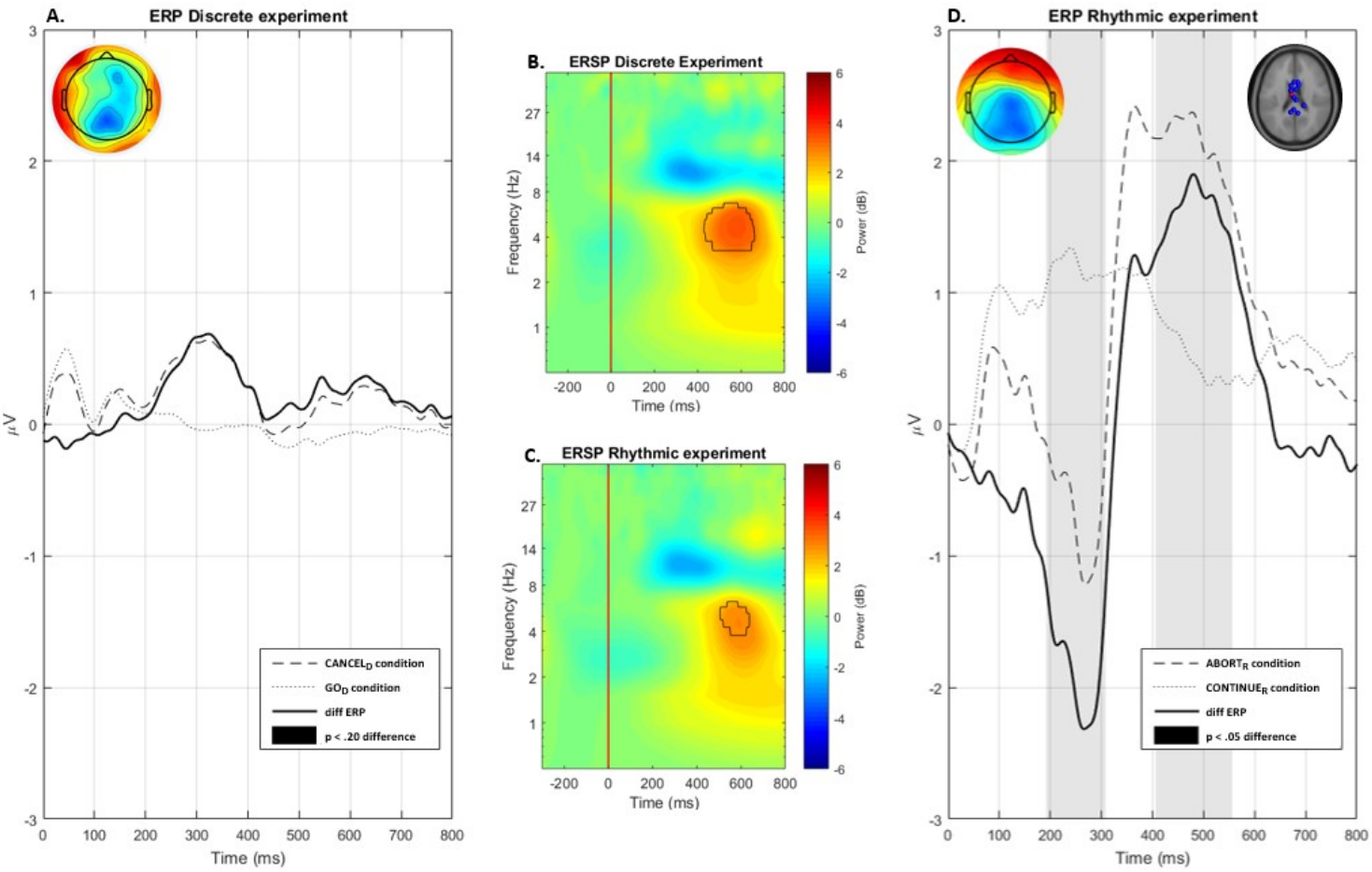

Fig.5: **Rhythmic chosen component (IC–R) analysis**

Panel A*: IC–R ERP (grand–average) in the discrete experiment, showing difference between GO_D and $CANCEL_D$ conditions.* ***Panel D****: IC–R ERP (grand–average) in the rhythmic experiment, showing difference between $CONTINUE_R$ and $ABORT_R$ conditions. $CANCEL_D$ and $ABORT_R$ conditions topographical maps of the IC–R components were computed in the channel space at the N2 peak latency. Equivalent current model of the participants' IC–Rs is also portrayed.*

Panel B–C*: IC–R ERSP maps computed in the discrete $CANCEL_D$ (B) and rhythmic $ABORT_R$ (C) conditions. Red line: STOP signal latency. Black line: region of significant activation ($p < .05$, corrected for multiple comparisons).*

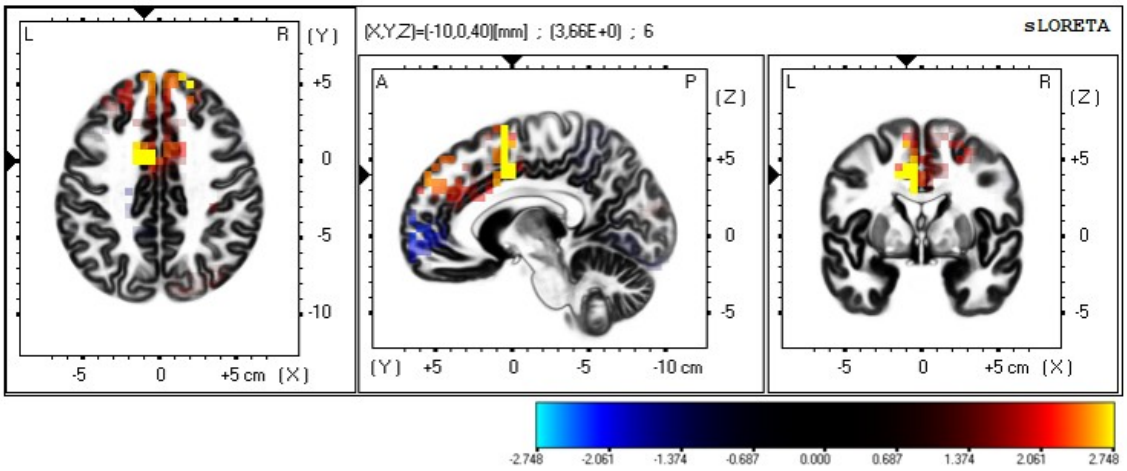

Fig.6: Source localization analysis: IC–D versus IC–R

The estimated sLORETA images showing statistical differences (t–values, two–tailed) between IC–D and IC–R for three orthogonal brain slices (horizontal, sagittal, coronal). Maximum current source density voxels are represented with greater IC–D values in yellow and greater IC–R values in blue. Only the voxels that passed the p value threshold (p < .01, corrected for multiple comparison) are shown in color.

Table.1: **Summary of significant results from whole-brain sLORETA estimation comparisons between IC-D and IC-R**

Lobe	Region	BA	*X*	*Y*	*Z*
Discrete experiment					
Limbic	Cingulate Gyrus	24	–10	0	40
	Cingulate Gyrus	32	–15	5	45
Frontal	Medial Frontal Gyrus	6	–10	5	55
	Superior Frontal Gyrus	6	–10	5	60
Rhythmic experiment					
Sub–lobar	Insula	13	–35	–25	5
Frontal	Middle Frontal Gyrus	9	55	15	30
	Medial Frontal Gyrus	10	–5	60	5
Limbic	Anterior cingulate	24	5	30	–5
	Anterior cingulate	32	5	35	0